JOURNAL OF APPLIED ELECTROCHEMISTRY 13 (1983) 147–155

The electrochemical formation of graphite–bisulphate intercalation compounds

L.E.A. BERLOUIS, D. J. SCHIFFRIN

Wolfson Centre for Electrochemical Science, Chemistry Department, The University, Southampton SO9 5NH, UK

Received 11 January 1982; revised 10 June 1982

The intercalation of bisulphate ion in graphite has been studied. Oxidation occurs in two stages, at 0.9V and 1.8V versus NHE, but the formation of thermally expandable compounds is associated with the second oxidation process. The first oxidation process is associated with the formation of a lower order of intercalation compound. The transport of HSO_4^- between the graphite planes is diffusion controlled and the diffusion coefficient value estimated is in the range of 0.3 to 2.8 x 10^{-6} cm^2 s^{-1} which indicates that the intercalated ions can move quite freely between the graphite planes. The oxidation of the graphite flakes in a fluidized bed electrode was studied by AC and voltammetric techniques. Good interparticle contact was achieved when a slight compressive load was applied and fluidization resulted in a large decrease of the solid phase resistance of the bed electrode.

Nomenclature

A	electrode area
C_i^0	HSO_4^- concentration corresponding to the i intercalation compound
$C_{(\infty, t)}$	HSO_4^- concentration in bulk graphite
$C_{(x, 0)}$	initial HSO_4^- concentration in graphite at any distance from the surface
C_{Ox}, C_R	bulk concentrations of the oxidised and reduced species of a redox couple in solution
D_{Ox}, D_R	diffusion coefficients of oxidised and reduced species of a redox couple in solution
F	faraday constant
n	number of electrons involved in a redox process
R	gas constant
R_e	effective resistance of the solution inside the bed
R_s	solid phase resistance of a bed electrode
t	time
T	absolute temperature
σ	Warburg coefficient

1. Introduction

The existence of compounds of graphite has been known for a long time [1], and of these, the lamellar complexes have been the most widely studied. The bonding between the flat graphite aromatic layers is rather weak and allows the insertion of simple chemical compounds giving rise to the formation of intercalates [2]. The stoichiometry of these is determined in principle by the requirements of formation of the corresponding sublattices, and the number of graphite layers separating each sublattice. In the case of the sulphuric acid lamellar complex the maximum stoichiometry corresponds to $C_{24}^+HSO_4^-$ [3]; the compound formed is known also to contain undissociated H_2SO_4 and the stoichiometry of this graphite salt is $C_{24}^+HSO_4^- \cdot 2.5H_2SO_4$ [4].

Increasing uses are being found for intercalation compounds; for instance, graphite–bisulphate is a very good catalyst for a range of esterification reactions performed at room temperature [5, 6]. Bromination reactions with graphite–bromine compounds have been described [6] and cetal formation and nitration reactions are known to occur [7]. Some recent developments [8] have shown the possibility of use of graphite–bisulphate as the positive electrode in secondary battery technology and the use of dilute sulphuric acid as an electrolyte has been suggested [9]. In the metallurgical industry, these compounds have been

0021–891X/83/020147–09$03.48/0

employed as expandable materials in insulating topping mixtures. On heating, intercalated graphites are known to increase in volume up to 300 times [10]. The resulting open structure has good insulating properties, which are used in the foundry industry to control the ingot solidification rate of the hot top. The graphite–bisulphate compound has been prepared by chemical oxidation in sulphuric acid using a variety of oxidizing agents, such as Mn^{3+}, $KMnO_4$, HNO_3, CrO_3 and others [1]. The oxidizing agents themselves are not intercalated and therefore the oxidation can be performed electrolytically [1, 11]. The purpose of this work was to study the general characteristics of the electrochemical oxidation process, and the feasibility of using a packed or semi-fluidized bed approach [12] for the bulk electrochemical oxidation of graphite to yield the thermally expandable forms [10].

2. Experimental procedure

Flake natural graphite from Madagascar was employed in all the experiments. Two different electrode configurations were used in this work: (1) For the electrochemical characterization of the material, solid pellets obtained by high pressure compaction of the flakes was used, and (2) A bed electrode made up of free graphite flakes was employed for the bulk electrochemical oxidation studies. The pellets were prepared by compressing the flakes under a total compressive force of 30 Tons,* in a die of 2.8 cm diameter. The pressure was maintained for 5 minutes and the electrical resistance across the pellet was less than 0.01 Ω. The circular pellets were cut in sections with the aid of a small saw and the sides were covered with acid resistant insulating masking enamel. Electrical contact was made with a copper wire inserted at one end of the electrode, and electrical continuity was ensured with silver paint. The electrode surface was polished with 1200 grit emery paper before each measurement and a conventional three electrode cell was employed. A Hi-Tek DT 11005 potentiostat with a Hi-Tek PPR1 waveform generator and a Bryans 26000 x–y recorder was used in the voltammetric work.

* 1 ton = 9.80665×10^3 newtons.

Figure 1 shows the flow cell used in the packed/semi-fluidized bed experiments. The working electrode comprised the bed of graphite flakes (length ≈ 3.0 cm) with a platinum gauze feeder electrode (40 strands per square inch) placed at the bottom of the bed. A 4.0 cm length of the flow cell prior to the electrode compartment was filled with glass ballotini to ensure a smooth velocity profile in the solution entering the bed. The counter electrode was a platinum spiral placed downstream and the reference electrode was a saturated mercury–mercurous sulphate saturated K_2SO_4 electrode (E_{rev} = 0.616 V versus NHE).

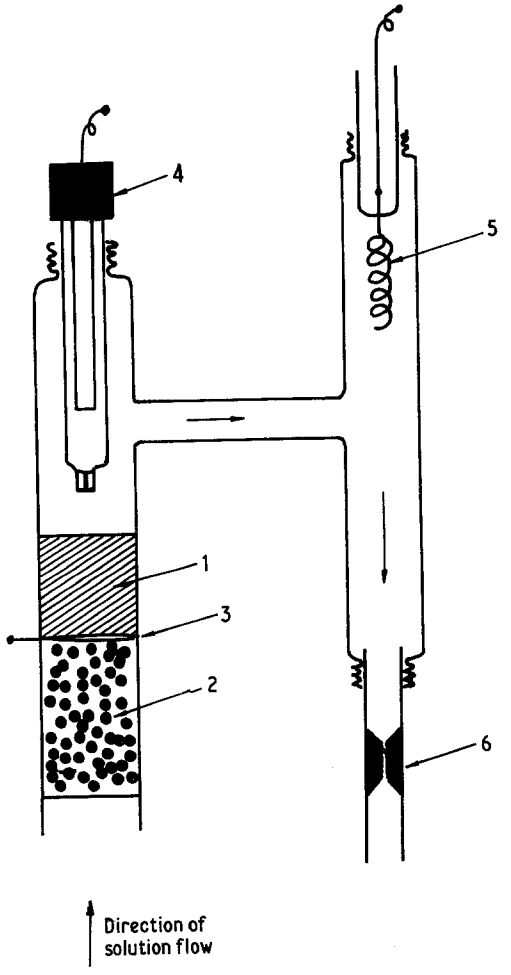

Fig. 1. Cell used for the fluidised bed experiments. (1) Bed of graphite flakes; (2) glass ballotini; (3) platinum gauze feeder electrode; (4) reference electrode; (5) platinum counter electrode and (6) capillary for controlling the flow rate.

The solutions were deaerated in a reservoir by bubbling nitrogen through them for about half an hour, and were kept under a slight overpressure of nitrogen. The solution flow rate was controlled by a capillary at the end of the flow line and was kept constant to within 0.3% during the course of the experiment by the nitrogen overpressure in the reservoir which served to maintain a constant hydrostatic head. The flow rate through the capillary was calibrated by measuring the volume delivered for a given time, using a measuring cylinder.

The cell used for the compressed bed experiments is shown in Fig. 2. Starting from a bed with a rest length of 3.0 cm, and using the plunger–syringe arrangement, the bed was compressed to different lengths i.e., 2.4, 2.0 and 1.75 cm. The a.c. impedance was measured by phase sensitive rectification of the current output of the potentiostat used for controlling the bed potential. The phase sensitive detectors and potentiostat used for this study were built from operational amplifiers [13] and the in-phase and quadrature components of the current were integrated with a Hi-Tek digital integrator.

The a.c. signal applied to the cell had an amplitude of 1.5 mV and a Brookdeal 9743 oscillator provided the input signal to the potentiostat as well as the in-phase and quadrature reference signals for the phase sensitive detectors.

The temperature in all experiments was 20 ± 2° C and all the results were referred to the normal hydrogen electrode (NHE) potential scale.

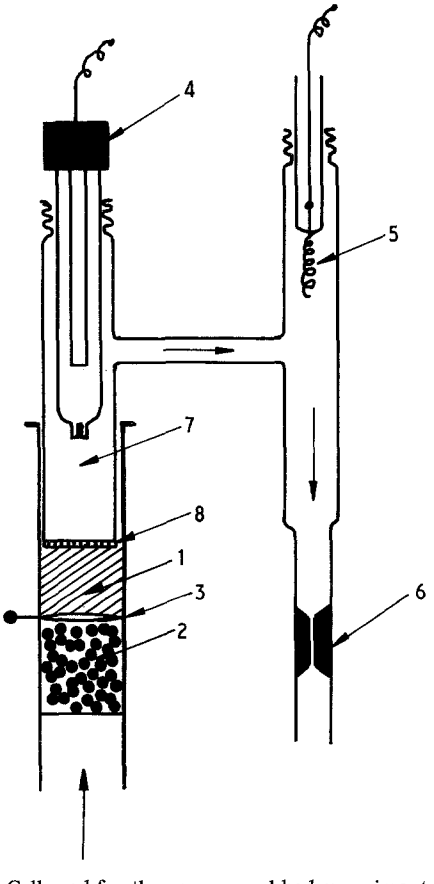

Fig. 2. Cell used for the compressed bed experiments. (1) Bed of graphite flakes; (2) glass ballotini; (3) platinum gauze feeder electrode; (4) reference electrode; (5) platinum counter electrode; (6) capillary for controlling the flow rate; (7) 10 cm^3 syringe and (8) nylon mesh fixed at the bottom of the open syringe plunger.

3. Results

Although the current densities measured were not very reproducible when different pressed samples were studied, the potentials of the oxidation and reduction peaks were reproducible. This result is expected for electrodes obtained by compression of an inhomogeneous powder. Therefore, the current densities quoted must not be taken to represent the values for the free flakes in a suspension with good particle interconnection.

Figure 3 shows some typical linear sweep voltammetry results. It is to be noted that although the potential for the second oxidation process is similar to that reported by Beck *et al.* [11] for the oxidation of graphite in sulphuric acid solution, we also find an oxidation process at less positive potentials; it is a high current density process and leads to a plateau region over 800 mV. Figure 4 shows the HSO_4^- ion concentration dependence of the *I–E* response while the influence of the proton concentration on the second oxidation process is shown in Fig. 5.

The first oxidation wave occurring at ~ 0.9 V has a sweep rate dependence characteristic of a diffusionally controlled process, i.e., the peak current is proportional to (sweep rate)$^{1/2}$.

The impedance results with planar electrodes are indicative also of a diffusionally controlled process in the potential region of the first anodic peak (Figs. 6 and 7) [11]. In order to determine

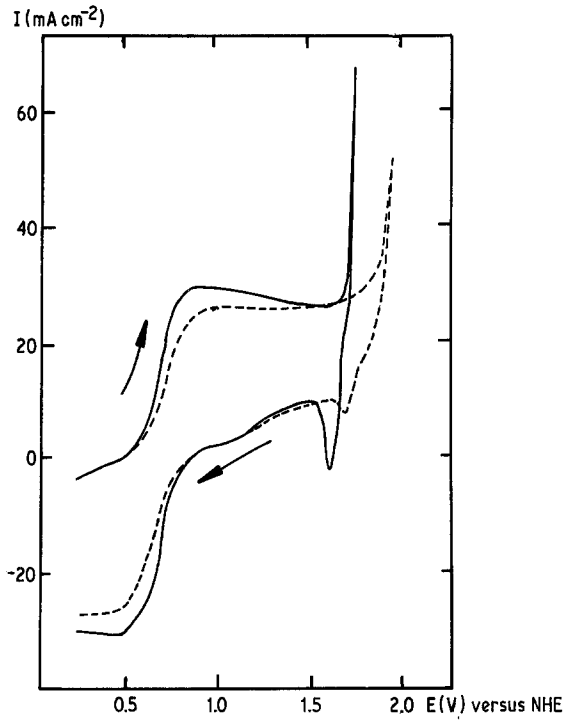

Fig. 3. Linear sweep voltammetry of high pressure compacted graphite flake electrode: — — — — 6 mol dm^{-3} $NaHSO_4$; ———— 6 mol dm^{-3} H_2SO_4. Sweep rate 0.02 V s^{-1}.

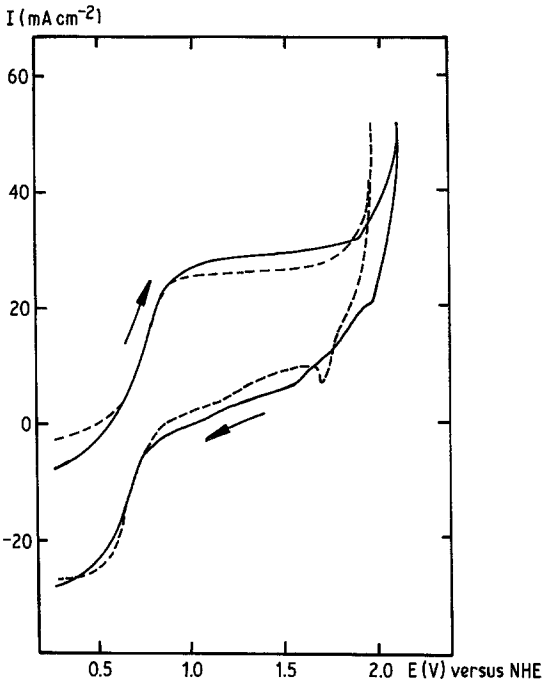

Fig. 4. Linear sweep voltammetry of a high pressure compacted graphite flake electrode in $NaHSO_4$ solutions of different concentration ———— 1 mol dm^{-3} $NaHSO_4$, — — — — — 6 mol dm^{-3} $NaHSO_4$.

the true geometrical electrode area, the impedance spectrum of a planar electrode in contact with a 10^{-2} mol dm^{-3} aqueous solution of the $Fe(CN)_6^{3-}$/$Fe(CN)_6^{4-}$ couple was measured and is shown in Fig. 8. The supporting electrolyte used was 0.5 mol dm^{-3} Na_2SO_4. The results were treated according to the Randles equivalent circuit [14] and from the measured Warburg coefficient:

$$\sigma = \frac{RT}{n^2F^2A2^{1/2}}\left(\frac{1}{C_{Ox}D_{Ox}^{1/2}} + \frac{1}{C_RD_R^{1/2}}\right) \quad (1)$$

the electrode area was calculated, and was found to coincide with the measured area. The diffusion coefficient values of the ferro- and ferricyanide ions used for this calculation were 4.7×10^{-6} cm^2 s^{-1} and 5.3×10^{-6} cm^2 s^{-1} respectively [15].

Impedance analysis on the bed of graphite flakes was carried out as before, using a 10^{-2} mol dm^{-3} aqueous solution of $Fe(CN)_6^{3-}$/$Fe(CN)_6^{4-}$ in 0.5 mol dm^{-3} Na_2SO_4, at the reversible potential of the hexacyanoferrate redox couple on graphite. Flow rates in the range 3–14 cm^3 min^{-1} were used and the impedance spectrum at each flow rate was recorded. The variation of the bed impedance with flow rate is shown in Fig. 9.

A computer fitting procedure was used to fit all the experimental results based on the one-dimensional transmission line model for a porous bed electrode [13, 16] (Fig. 10). A typical result for the compressed bed experiments is shown in Fig. 11, where the drastic decrease of the bed impedance caused by compression can be clearly seen.

4. Discussion

The voltammetric results show that the acid sulphate ion is not involved in the rate determining step of initial graphite oxidation, since a sixfold increase in current should have been easily observed in the results shown in Fig. 4 for the first oxidation wave. The dissimilarity in potential for the first oxidation wave between Beck's work [11] and the present one could be linked with the different methods of electrode preparation. Beck used a polypropylene/natural graphite mixture to prepare his electrode, whereas here pure natural

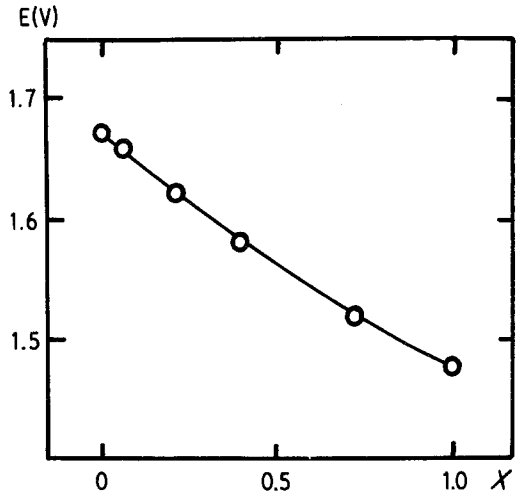

Fig. 5. Oxidation potential of a high pressure compacted graphite flake electrode for different H^+ ion concentrations at a constant HSO_4^- concentration of 6 mol dm^{-3}. The potentials correspond to a current density of 0.05 A cm^{-2} for linear sweep experiments. Sweep rate 0.02 V s^{-1}. The results correspond to mixtures of composition X6 mol dm^{-3} H_2SO_4 + $(1-X)$6 mol dm^{-3} $NaHSO_4$.

graphite in a highly compacted form was employed. The first oxidation process though, is diffusionally controlled (Figs. 7 and 8) and corroboratory evidence for this was obtained from current–time transients. Figure 12 shows potential step results for the planar graphite electrode in 6 mol dm^{-3} H_2SO_4 acid. At potentials well beyond the first oxidation peak, but before the second oxidation process, the current is a

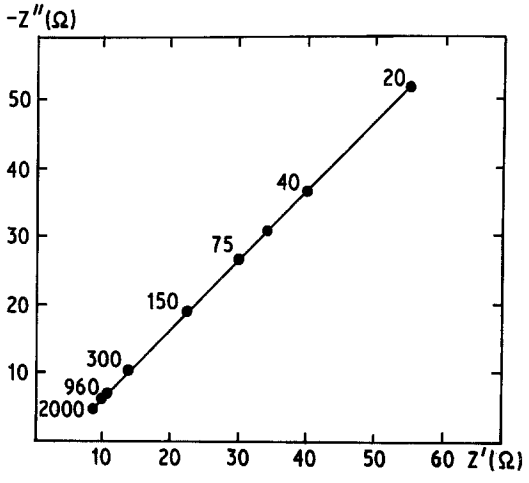

Fig. 6. Impedance plot for a planar high pressure compacted graphite flake electrode in 0.5 mol dm^{-3} Na_2SO_4. Frequencies in Hz are indicated in the figure. The electrode was at the rest potential, 0.66 V versus NHE.

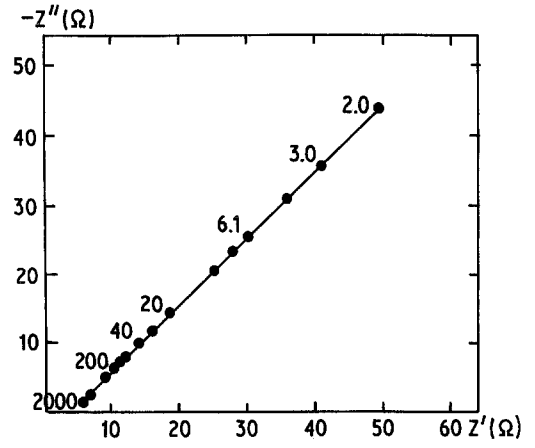

Fig. 7. Impedance plot for a planar high pressure compacted graphite flake electrode in 0.5 mol dm^{-3} H_2SO_4. Frequencies in Hz are indicated in the figure. The electrode was at the rest potential, 0.76 V versus NHE.

linear function of $t^{-1/2}$, as expected for diffusionally controlled intercalation. For semi-infinite planar diffusion, the current–time relationship is [17]

$$i = \frac{nFC_i^0 D^{1/2}}{\pi^{1/2} t^{1/2}}. \qquad (2)$$

Equation 2 applies for a diffusional field established with the boundary and initial conditions:

$$C_{(0,t)} = C_i^0, \qquad C_{(\infty,t)} = 0, \qquad C_{(x,0)} = 0. \qquad (3)$$

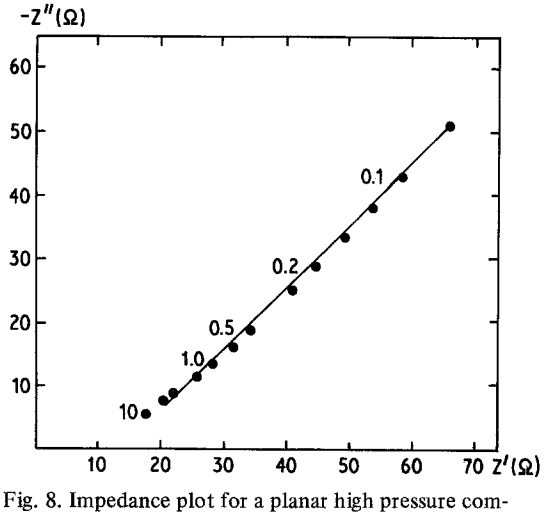

Fig. 8. Impedance plot for a planar high pressure compacted graphite flake electrode in contact with a 0.01 mol dm^{-3} $Fe(CN_6)^{3-}/Fe(CN_6)^{4-}$ redox couple in 0.5 mol dm^{-3} Na_2SO_4 at the reversible potential (E = 0.431 versus NHE).

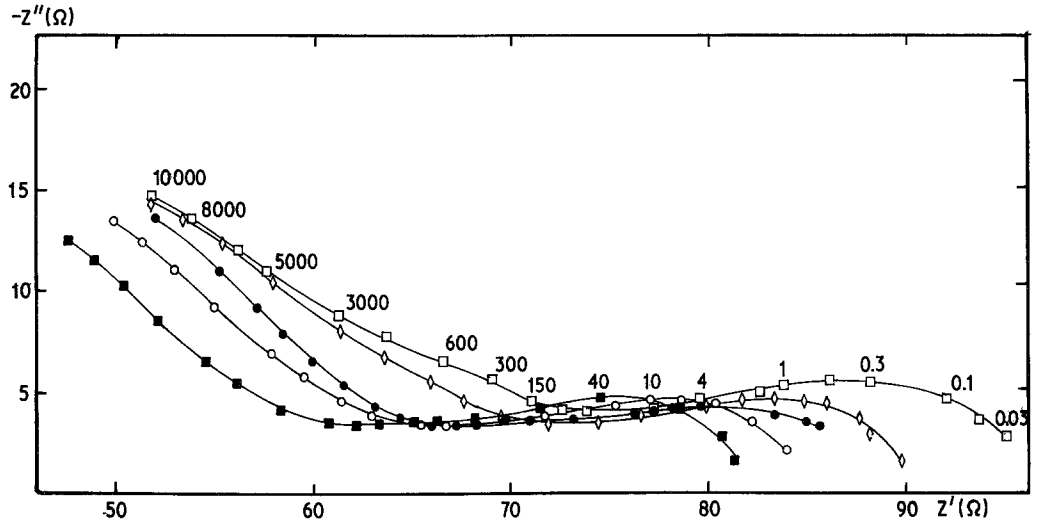

Fig. 9. Impedance plot for an unconsolidated bed of graphite flakes as a function of flow rate at the reversible potential ($E = 0.431 \pm 0.003$ V versus NHE). With no flow, bed length = 2.0 cm; supporting electrolyte = 0.5 mol dm^{-3} Na_2SO_4, redox couple = 0.01 mol dm^{-3} $Fe(CN_6)^{3-}/Fe(CN)_6^{4-}$. Flow rates (cm^3 min^{-1}); •, 3.66; ▪, 6.85; ◇, 7.84; ○, 11.94 and □, 13.2.

C_i^0 is the concentration of HSO_4^- corresponding to the intercalation compound formed; although the $C:HSO_4^-$ ratio for the first oxidation is not known, the possible limits are $C_{24}^+HSO_4^-$ and $C_{72}^+HSO_4^-$ [1–4]. Therefore, taking the approximate density of the compounds as equal to graphite (~ 2 g cm^{-3}) the C_i^0 values for the C_{24}^+, C_{48}^+ and C_{72}^+ compounds are 6.9, 3.5 and 2.3 mol dm^{-3}, respectively. From the results in Fig. 12, the range of diffusion coefficients calculated is from 3.1×10^{-7} to 2.8×10^{-6} cm^2 s^{-1}. These results differ from those of Beck *et al.* [9, 11] who found a value of 7×10^{-8} cm^2 s^{-1} for the diffusion of sulphate and 3.2 to 4.5×10^{-9} cm^2 s^{-1} for the diffusion of perchlorate in graphite from transient and steady state measurements across pressed pellets with polypropylene binding. In their work, the transversal geometrical dimensions of the pressed pellet were used as the diffusional length. The pressing process employed resulted in an orientation of the flakes parallel to the surfaces and as a consequence, the real diffusional path is much greater than the geometrical overall diffusional thickness. This probably accounts for the difference in the values of the diffusion coefficients found. The results presented here are not dependent on any assumption regarding the real diffusional length and probably represent more accurately the value for the diffusions of the HSO_4^- ion within the graphite planes. In addition, the actual active electrode surface may be different due to the use of a binder, and the time scale used for the calculation of the diffusion coefficient is quite different. In the work of Beck *et al.* [11] results at diffusion times greater than 100 s were used whereas the present work refers to a maximum electrolysis time of ~ 2 s. The large disparity in the value of D may be therefore, a consequence of the analysis of different processes occurring at different times.

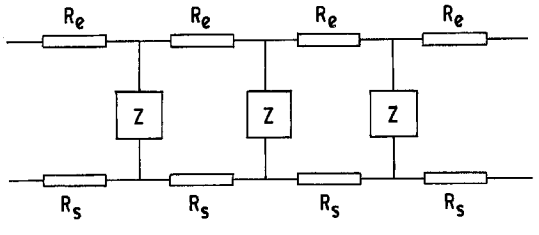

Fig. 10. One dimensional transmission line model for a porous electrode used in the analysis of the bed impedance results, R_e = solution resistance per unit length in porous electrode; R_s = solid phase resistance per unit length; Z = interfacial reaction impedance.

It is interesting to note that the diffusion coefficient values calculated are, at the most, one order of magnitude lower than those corresponding to aqueous solutions. These high values are quite unusual for solid state diffusion and show that the intercalated ions can move quite freely

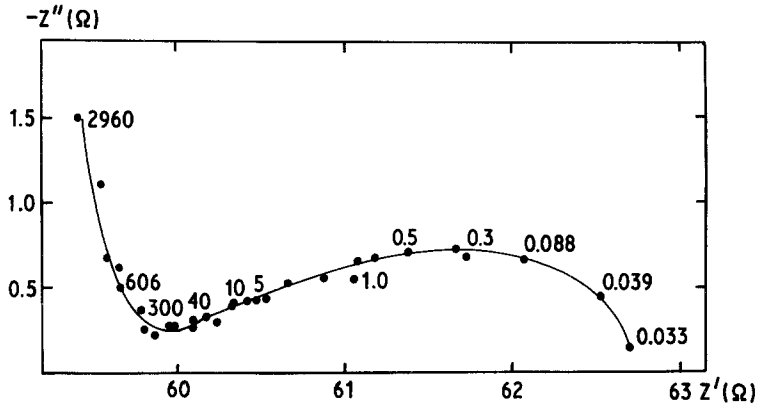

Fig. 11. Impedance plot for a compressed graphite flake bed electrode at the reversible potential. Length of compressed bed = 1.75 cm; uncompressed bed length 3.0 cm; flow rate 12.5 $cm^3\ min^{-1}$; supporting electrolyte — 0.5 mol dm^{-3} Na_2SO_4; redox couple = 0.01 mol dm^{-3} $Fe(CN)_6^{3-}/Fe(CN)_6^{4-}$.

between the graphite planes. Therefore, the first peak corresponds to the diffusion of either SO_4^{2-} or HSO_4^- through the graphite lattice and the surface concentration of the diffusing species is determined by the stoichiometry of the corresponding graphite salt. In this way, the bulk concentration of SO_4^{2-} or HSO_4^- in the concentration ranges studied will not determine the rate of intercalation.

The above discussion is based on the idea that the first oxidation peak is associated with the formation of a lower order of intercalation compound. The possible involvement of quinone surface groups in the anodic oxidation of carbon and graphite surfaces has been previously observed by Blurton [18], Randin and Yeager [19] and Lowde *et al.* [20], among others. For the surface processes, broad oxidation peaks occur at 0.7 V versus NHE [18] whereas the reduction of electrochemically oxidised carbon occurs at ~ 0.5 V. The potentials of the quinone–hydroquinone and 1-2 naphthoquinone redox couples occur at 0.6995 and 0.547 V respectively and this has been taken as indicative of the involvement of the quinone systems in the redox properties of carbon surfaces [19]. Indeed, the presence of these types of surface groups has been known for a long time [21], but cannot account for our experimental results. At the sweep rates employed in this work, the current densities observed at the first peak were of the order of 30 mA cm^{-2}, whereas the results for a true surface redox process gave peak currents of ~ 0.4 mA cm^{-2} [18], i.e., two orders of magnitude lower than those observed in this work. Furthermore, a surface redox process cannot lead to a diffusionally controlled response as observed here (Figs. 6, 7 and 12) and it must be concluded that a bulk process is occurring. The differences in behaviour of natural graphite as used in this work, and synthetic materials [18], is very striking and is most likely due to the size of the graphite crystallites. In the case of the synthetic materials, bulk diffusion for the intercalation process will be severely hindered by orientational mismatch of the crystallites.

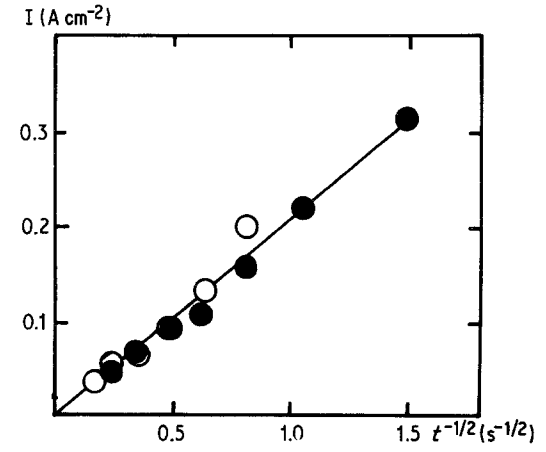

Fig. 12. Current–time transients for a planar high pressure compacted graphite flake electrode in 6 mol dm^{-3} H_2SO_4 for potentiostatic potential step experiments. Starting potential = 0.24 V; potential stepped to; •, 1.24 V and ○, 1.44 V; versus NHE.

The nature of the second oxidation process is still not clear, but it is dependent on the H^+ ion concentration, since the results shown in Fig. 5 correspond to constant HSO_4^- ion concentration. It is usually considered that the oxidation process refers only to the intercalation of an anion and the formation of a positive charge residing on the graphite planes. It is more likely though, that the intercalation process is accompanied by the oxidation of either keto or phenolic groups as part of

the intercalation process [18]. The presence of these types of functional groups gives a reasonable explanation for the shift in oxidation potential with pH.

The formation of expandable graphite occurs only when the process is performed in the second oxidation region. This was observed by performing chemical oxidations with a variety of reagents (H_2O_2, $K_2S_2O_8$, $KMnO_4$) and expandable forms were only obtained when the redox potential corresponded to the onset of the second oxidation process. To perform this reaction, a fluidized bed arrangement seemed a most suitable approach for industrial scale-up. The characterization of the bed in terms of solid phase resistance, solution resistance and active area of bed per unit electrode length was carried out using the a.c. impedance technique previously described.

The effect of flow rate on the bed is clearly seen from the results in Table 1. The active area decreases with increasing flow rate due to the effect of decreasing interparticle contact. The values are extremely low, showing that the bed of graphite flakes used in this configuration was unsuitable for oxidising graphite electrolytically. The solid phase resistance, R_s, increases with flow rate, again due to a decrease in interparticle contact as the flow rate was increased. The effective solution resistance inside the bed, R_e, shows little variation at flow rates higher than 4 $cm^3\ min^{-1}$ showing that the electrolyte path through the bed at these higher flow rates reaches a constant value.

Table 2 shows the effect of changing the electrode length on the solid and electrolyte phase resistances. As the electrode length increases, R_s (measured per unit length of electrode) decreases due to the effect of compression of the flakes at the bottom of the bed by the weight of the graphite in the column above it. R_e, on the other hand, increases with electrode length, as the solution path through the bed increases.

Table 1. Parameters calculated for the unconsolidated bed of graphite flakes as a function of solution flow rate. Bed length 2.0 cm

Flow ($cm^3\ min^{-1}$)	*Area* ($cm^2\ cm^{-1}$)	R_s ($\Omega\ cm^{-1}$)	R_e ($\Omega\ cm^{-1}$)
3.6	0.33	0.39	44
5.9	0.31	0.57	37
7.8	0.27	0.59	39
11.9	0.29	0.61	38
13.2	0.22	0.80	39

Table 2. Parameters for graphite bed electrodes of different heights. Flow 13.2 $cm^3\ min^{-1}$

Electrode length (cm)	R_s ($\Omega\ cm^{-1}$)	R_e ($\Omega\ cm^{-1}$)
3.6	0.77	46
3.0	0.80	38
2.7	0.96	37

Table 3 shows the results obtained from the compressed bed experiments, using the cell shown in Fig. 2. It is evident, from the values of area and solid phase resistance, that the effect of compressive loads on the bed leads to a great increase in interparticle contact. The solution resistance, though, *increases* with compression; this is evidence for the increased effective path length of the electrolyte as the contact between flakes is enhanced.

The conclusions reached from the a.c. impedance analysis were verified in the linear voltage sweep experiments carried out on both expanded and compressed beds in a 2 mol dm^{-3} H_2SO_4/4 mol dm^{-3} $NaHSO_4$ aqueous mixture. As can be seen from Fig. 13, almost no oxidation of the graphite can be observed in the expanded beds, whereas on compression, the oxidation of graphite can be clearly seen.

The current–potential curves for the compressed bed are different from the voltammograms for the plane electrode shown in Figs. 3 and 4. It must be realized that these two experiments refer to two different conditions; for the planar electrode, the current–potential relationship is solely determined by solid phase diffusion. For the bed electrode, the current–potential curve (Fig. 13) reflects not only the electrochemical process occurring on each graphite flake but also the potential distribution across the bed due to ohmic

Table 3. Parameters for a compressed bed as a function of degree of compression. Flow 12 $cm^3\ min^{-1}$

Compressed bed length (cm)	*Area* ($cm^2\ cm^{-1}$)	R_s ($\Omega\ cm^{-1}$)	R_e ($\Omega\ cm^{-1}$)
Initial = 3.0 cm	0.25	0.78	37
2.4	1.14	0.16	42
2.6	2.89	0.10	41
1.75	3.40	0	42

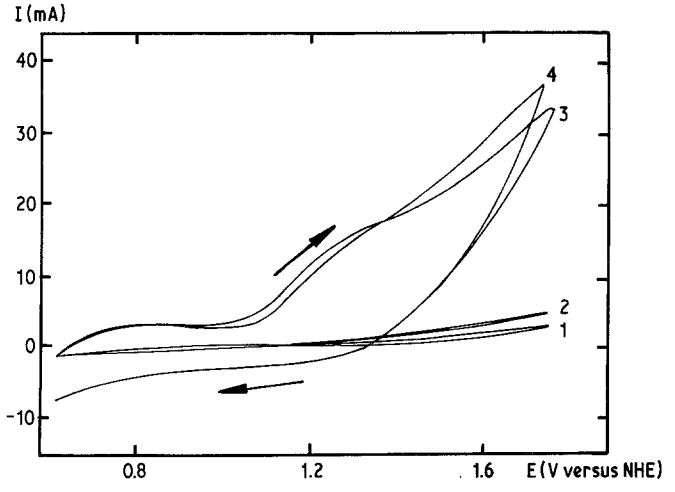

Fig. 13. Linear sweep voltammetry of a graphite flake bed electrode in 2 mol dm^{-3} H_2SO_4 + 4 mol dm^{-3} $NaHSO_4$ electrolyte. Sweep rate = 0.02 V s^{-1}. (1) Unconsolidated bed; flow rate 14 cm^3 min^{-1}, length 3.3 cm; (2) unconsolidated bed; flow rate 6 cm^3 min^{-1}, length 3.3 cm; (3) compressed bed, stationary solution, length 2.6 cm, initial length 3.3 cm and (4) same as 3 but with a bed length of 2.0 cm.

drop in both phases [22]. Therefore, the measured voltammetric curves will depend on the detailed potential distribution across the bed and the measured current represents an integral quantity. Nevertheless, the result shown in Fig. 13 is a very good indication of the enhancement of interparticle contact under slight compressive loads.

5. Conclusions

The intercalation of the HSO_4^- ion in graphite at potentials corresponding to the second oxidation wave results in thermally expandable forms. In the first oxidation region, the oxidation is diffusionally controlled, corresponding to the transport of HSO_4^- between the graphite planes. The impedance results show that fluidization of the graphite bed electrodes results in the loss of interparticle contact and it is likely that the flat geometry of the particles is detrimental to the establishment of electrical contact in the presence of upward flow through the bed. Slight compression of the bed increases the electrical continuity and electrolysis becomes possible under these conditions.

Acknowledgements

Helpful comments and suggestions by Professor G. J. Hills at Southampton University are gratefully acknowledged.

References

[1] G. R. Henning, *Prog. Inorg. Chem.* **1** (1959) 125.
[2] M. C. Robert, M. Oberlin and J. Mering, in "Chemistry and Physics of Carbon", Vol. 10, (edited by P. L. Walker and P. A. Thrower). Marcel Dekker, New York (1973) p. 141.
[3] J. J. Bottomley, G. S. Parry, A. R. Ubbeholde and D. A. Young, *J. Chem. Soc.* (1963) 5674.
[4] S. Aronson, S. Lemont and J. Weiner, *Inorg. Chem.* **10** (1971) 1296.
[5] J. Bertin, H. B. Kagan and Jean-Louis Lunche, *J. Amer. Chem. Soc.* **96** (1974) 8113.
[6] H. B. Kagan, *Pure and Appl. Chem.* **46** (1976) 177.
[7] J. P. Alazard, H. B. Kagan and R. Setton, *Bull. Soc. Chim. France* (1977) 499.
[8] R. Fujii, *Electrochem. Ind. Phys. Chem.* **40** (1972) 705.
[9] F. Beck and H. Krohn, Paper A14, 32nd I.S.E. Meeting, Dubrovnik/Cavtat, Yugoslavia (1981).
[10] H. Thiele, *Trans. Faraday Soc.* **34** (1938) 1033.
[11] F. Beck, H. Junge and H. Krohn, *Electrochim. Acta* **26** (1981) 799.
[12] A. K. P. Chu, M. Fleischmann and G. J. Hills, *J. Applied Electrochem.* **4** (1974) 331.
[13] L. E. A. Berlouis, Ph.D. Thesis, University of Southampton (1981).
[14] J. E. B. Randles, *Disc. Faraday Soc.* **1** (1947) 11.
[15] J. Wojtowicz and B. Conway, *J. Electroanalyt. Chem. Interfacial Electrochem.* **13** (1967) 333.
[16] R. de Levie, in 'Advances in Electrochemistry and Electrochemical Engineering', Vol. 6 (edited by P. Velahay). Interscience Publishers (1967) p. 329.
[17] A. J. Bard and L. R. Faulkner, 'Electrochemical Methods', John Wiley & Sons, New York (1980).
[18] K. F. Blurton, *Electrochim. Acta* **18** (1973) 869.
[19] T. P. Randin and E. Yeager, *J. Electroanal. Chem.* **58** (1975) 313.
[20] D. R. Lowde, J. O. Williams, P. A. Attwood, R. J. Bird, B. D. McNicol and R. T. Short, *J. Chem. Soc. Faraday Trans.* **I** (1979) 2312.
[21] V. A. Garten and D. E. Weiss, *Austr. J. Chem.* 8 (1955) 68.
[22] J. Newman and C. Tobias, *J. Electrochem. Soc.* **109** (1962) 1183.